Supplementary Information

Plasmon-modified dielectric Mie resonances from laser-synthesized Si@Au nanoparticles for photothermal therapy applications

A. V. Kondakova[a], D. U. Musaev[a,b], I. D. Kuchumov[a], K. A. Cherednichenko[c], G. A. Gruzdev[d], V. G. Yakunin[a], V. S. Belov[b], G. V. Tikhonowski[b], A. A. Popov[b,e], A. A. Novikov[c], S. M. Klimentov[b,e], A. A. Garmash[b] , A. V. Kabashin[*f] , V. Yu. Timoshenko[*a,b,g]

[a]*Lomonosov Moscow State University, Physics Dep., Leninskie Gory 1, 119991 Moscow, Russia*

[b]*MEPhI University, Institute of Engineering Physics for Biomedicine (PhysBio), 115409 Moscow, Russia.*

[c]*Oil & Gas Research Institute of the Russian Academy of Sciences, Russian Federation, Gubkina str. 3, 119333 Moscow, Russia*

[d]*Lomonosov Moscow State University, Biology Dep., Leninskie Gory 1, 119991 Moscow, Russia*

[e]*Department of Physics and Applied Mathematics, Vladimir State University named after A. G. and N. G. Stoletovs, 600000 Vladimir, Russia*

[f]*Aix-Marseille University, CNRS, LP3, Marseille, 13288, France*

[g] *Shenzhen MSU-BIT University, Faculty of Materials Sciences, Shenzhen, 518172, P.R. China*

**Corresponding authors: andrei.kabashin@univ-amu.fr and timoshen@physics.msu.ru*

1. SEM and TEM data

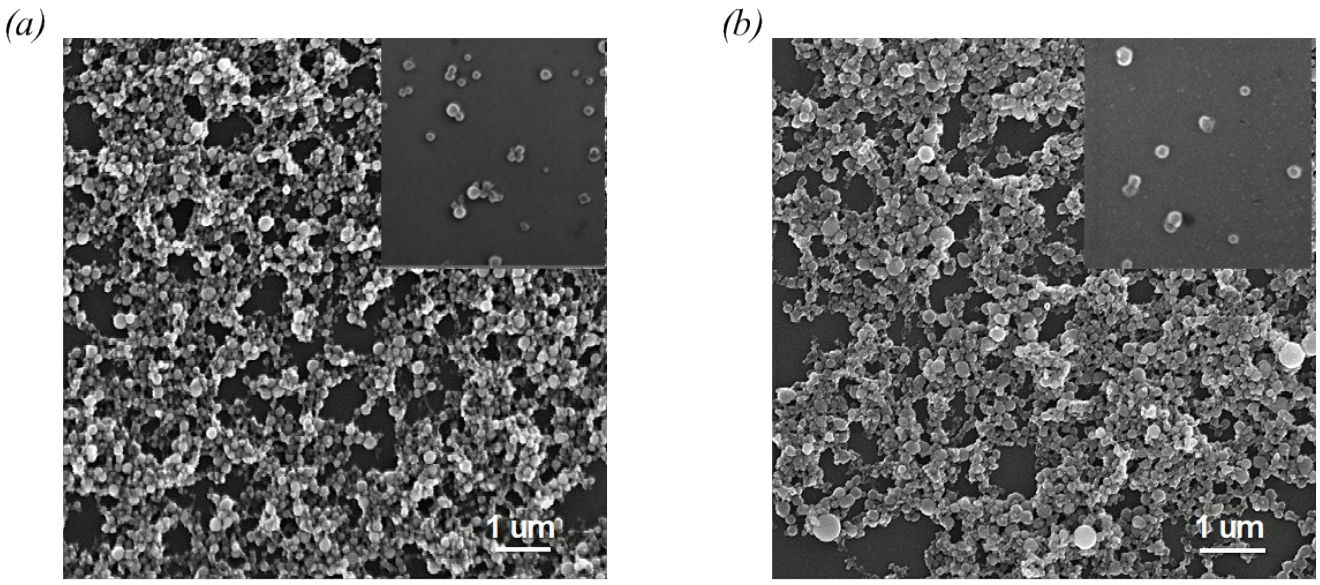

Figure S1. SEM images of (a) green-Si and (b) red-Si NPs, which were deposited from concentrated aqueous suspensions. Insets show SEM images obtained from the corresponding diluted suspensions.

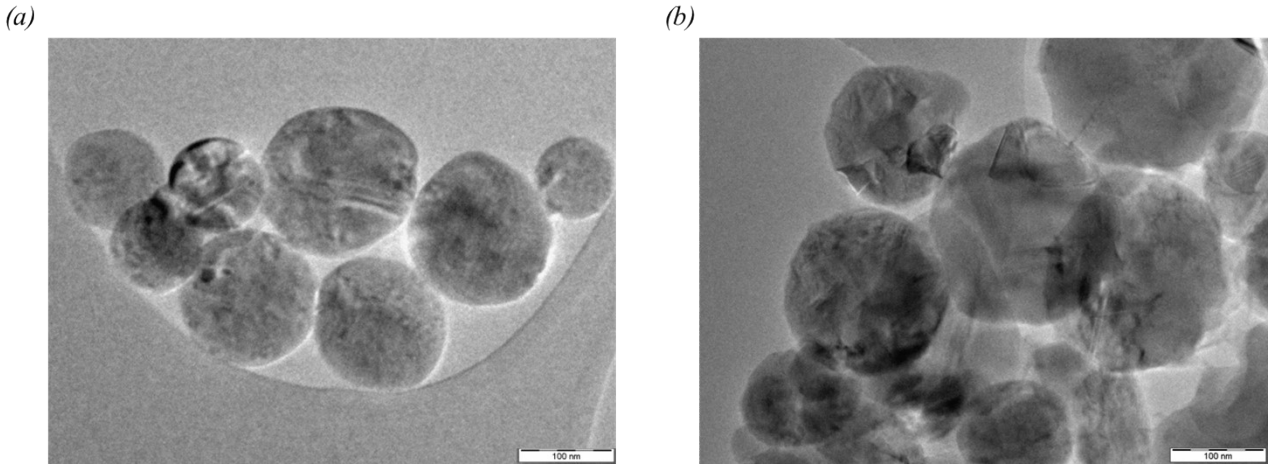

Figure S2. Typical TEM images of (a) green-Si and (b) red-Si NPs.

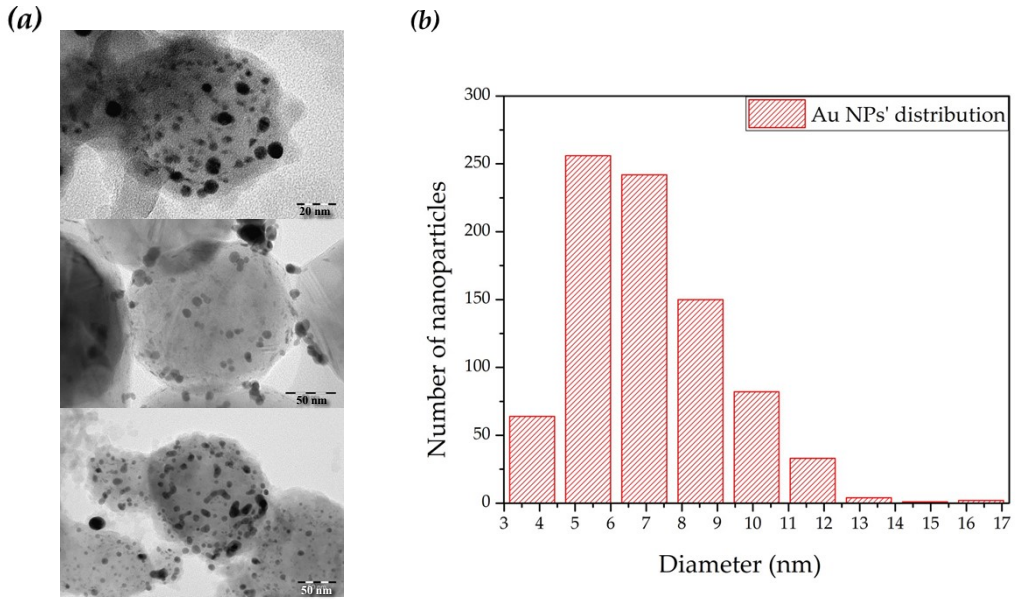

Figure S3. (a) Representative TEM images and (b) size distribution of Au NPs, which was obtained from these images.

2. Model and simulation results

Fig.S4(a) shows a model, which was used to simulate the electric field strength, optical absorption and scattering cross-sections of a Si NP. A problem of the light scattering and absorption by Si NP in water environment was solved numerically by using the Lumerical Finite Difference IDE software (ANSYS, Inc.). Spectral dependences of the refractive indices of silicon and water were taken from the Palik database. A light source was specified with an amplitude of the electric field of 1 V/m. The scattering (Q_{abs}) and absorption cross-sections (Q_{sca}) were calculated using numerical solutions of the Maxwell equation for given boundary conditions, by adding the averaged Poynting vectors and normalizing to the source intensity. The electric field strength was normalized to the source field for light wavelengths, which corresponded to the experimental conditions.

Figure S4(b) shows an example of the spatial distribution of the normalized modulus of the electric field in the cross-section of an isolated Si NP with a diameter of 170 nm upon irradiation with light at a wavelength of 810 nm. The field distribution corresponds to the Mie-scattering by a dielectric sphere for the condition of weak light absorption.

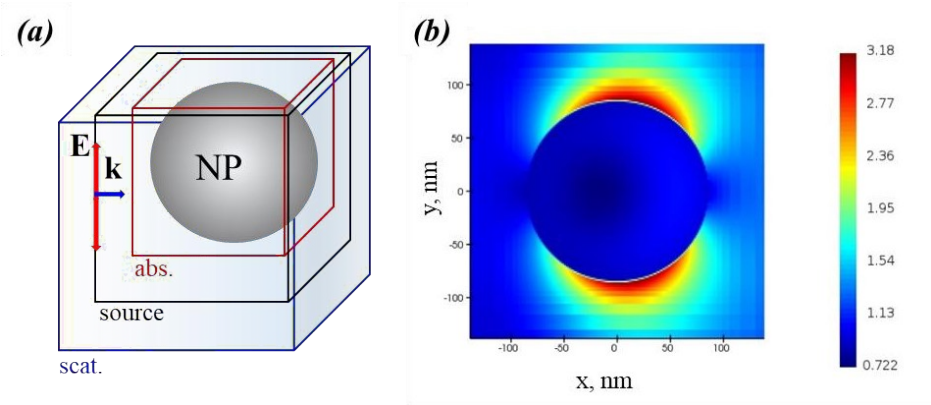

Figure S4. (a) Schematic representation of the geometry of simulations of the electric field distribution,absorption and scattering cross-sections of a NP; (b) cross-sectional electric field distribution for a Si NP in water environment.

Simulated spectra of the absorption and scattering cross-sections for Si NPs with different diameters varied from 90 to 170 nm are shown in Figure S5. It is seen that all dielectric resonances are nearly linearly shifted to the long-wavelength region with an increase in the NP' size. In this case, the absorption cross-section is smaller than the scattering cross-section. It is interesting that the peak wavelength of the magnetic dipole (MD) absorptionresonance coincides with the wavelength of the scattering peak and its position shifts almost linearly with the NP size see Fig. S2 (c). In this case, the peak value of the absorption cross-section for the MD mode remains practically unchanged, regardless of the NP diameter. At the same time, the amplitude of the absorption cross-section for the electric dipole mode (ED) of Si NPs increases in proportion to the NP diameter as it is shown in Fig. S5 (a, d).

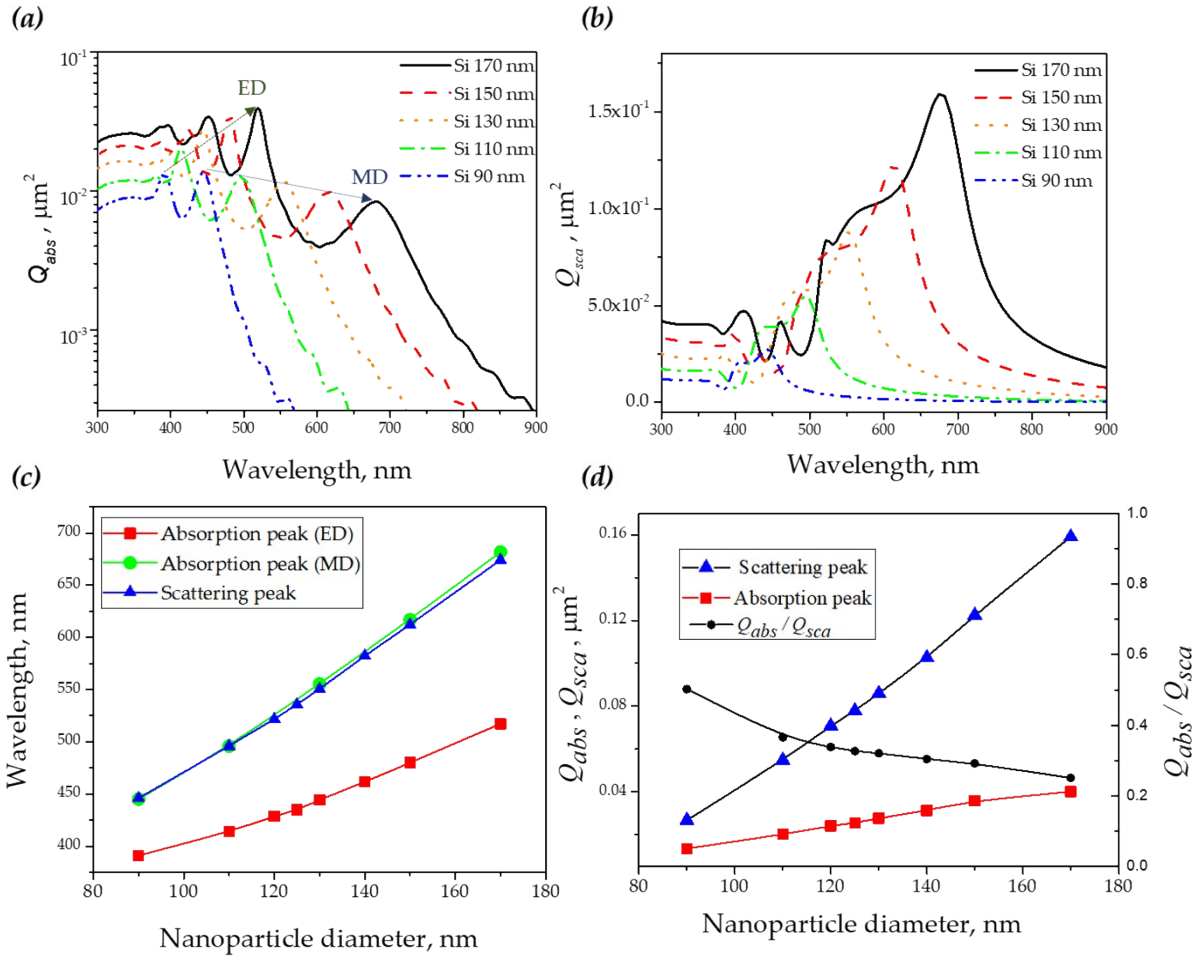

Figure S5. (a) Simulated spectra of the absorption cross-section and (b) scattering cross-sections of a single Si NP in water. The arrows indicate shifts of the electric dipole (ED) and magnetic dipole (MD) modes with increasing NP size; (c) dependences of the resonance wavelength on diameter of Si NP; (d) dependences of the cross-sections of absorption (red squares) and scattering (blue up-triangles) and their ratio (black circles) on diameter of Si NP.

Figure S6 shows cross-sectional maps of the spatial distribution of the electric field around silicon NPs of two types: “green”-Si (d=120 nm, top row) and “red”-Si (d=160 nm, bottom row). The field amplification was calculated during irradiation with lasers with wavelengths of green (panels a,d), red (panels b, e) and near-IR (panels c, f) ranges. For all wavelengths, the maximum gain in the electric field modulus remains close to 3, which is equal to the refractive index of silicon. For the considered Si NPs’ concentrations, the fields from neighboring nanoparticles do not affect each other.

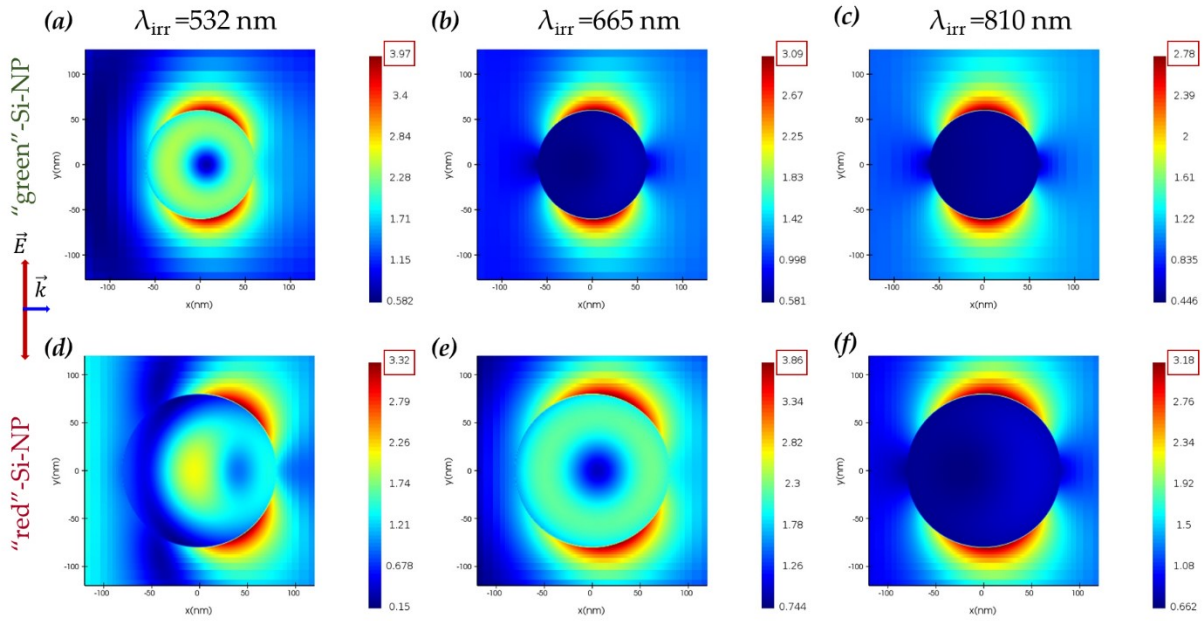

Figure S6. Simulated distributions of the electric field strength around (a-c) green- and (d-f) red-Si NPs under irradiation at 532 nm (a, d), 665 nm (b,e), 810 nm (c,f).

To simulate optical responses of ensembles of Si, Si@Au and Au NPs we consider 100 Si NPs with lognormal distributed sizes with parameters corresponding to the experimental samples of green- and red-Si NPs obtained via the size selection procedure from the laser ablated Si NP suspensions. Nanocomposite particles based on "green"-Si and "red"-Si cores with gold NPs with 10 nm in diameter were randomly distributed over their surfaces. The constant 10 nm diameter of Au NPs is chosen for simplicity reasons as well taking into account that the experimental size distribution of Au NPs (see Fig.S3b) corresponds the volume (mass) distribution centered near 9-10 nm. The amount of gold on the Si NPs' surfaces was about 5.1 and 3.4 at.% for the cases of green- and red-Si NPs, respectively. The latter values were chosen according to the experimentallymeasured ones (Table 2). The average distance between Si and Si@Au NPs was about 400 nm. When comparing the opticalproperties of different ensembles, the cross-sections were normalized to the number of Si NPs.

Figure S6 shows simulated distributions of the electric field for green- Si@Au (d=120 nm, top row) and red-Si@Au (d=160 nm, bottom row) Si@Au NPs in water. The field amplification depends on wavelength, and it is very different for the irradiation in the green (panels a, d), red (panels b, e) and near-IR (panels c, f) ranges. Under irradiation at 532 nm, the field amplification compared to the source field does not exceed 21 times for both geometries. The greatest enhancement is observed when irradiated with light with a wavelength of 665 nm, up to80 times for a larger NP (panel e).

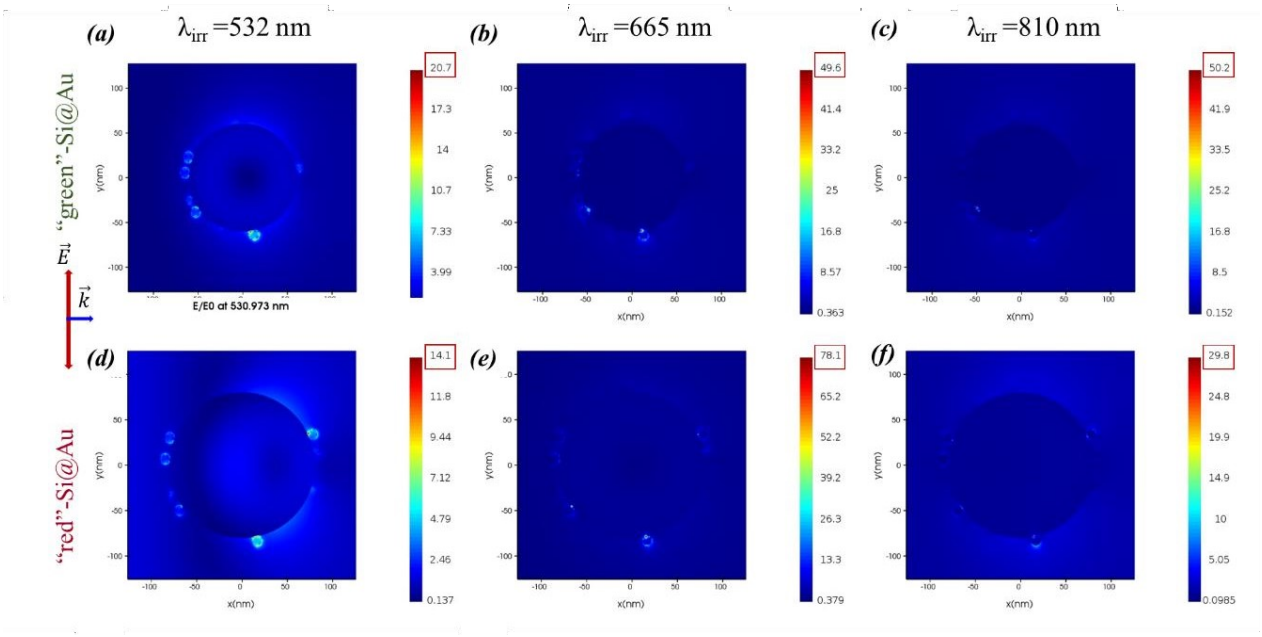

Figure S7. Simulated distributions of the electric field strength for green- Si@Au (a-c) and red-Si@Au (d-f) NPs under irradiation at 532 nm (a, d), 665 nm (b, e), and 810 nm (c, f).

3. Temperature transients for the experiments *in vitro*

Figure S8 shows temperature dependences in water solutions with *Paramecium caudatum* cells without and with added red-Si and red-Si@Au NPs. The initial heating rate during the first 20 seconds of temperature growth was about 0.4 °C/min for cells without NPs, 1.6 °C/min for cells with Si NPs and 3.4 °C/min for cells with red-Si@Au NPs.

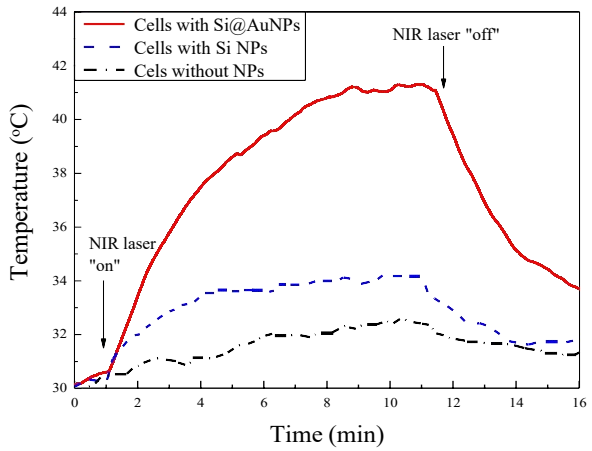

Figure S8. Experimental temperature transients for suspensions of *Paramecium caudatum* cells without NPs (black dash-dotted curve), with added red-Si NPs with mean diameter of 160 nm (blue dashed curve) and red-Si@AuNPs (red curve) under NIR irradiation at 830 nm with power of 1 W. The NPs' concentrations were about 0.5 mg/mL, and the suspension volume was 1.2 mL.